Gradient corrections to the kinetic energy density functional of a two-dimensional Fermi gas at finite temperature

B. P. van Zyl,[1] K. Berkane,[2] K. Bencheikh,[2] and A. Farrell[1]

[1]*Department of Physics, St. Francis Xavier University, Antigonish, Nova Scotia, Canada B2G 2W5,*

[2]*Département de Physique, Laboratoire de physique quantique et systèmes dynamiques, Université de Sétif, Setif 19000, Algeria*

(Received 2 December 2010; revised manuscript received 7 March 2011; published 31 May 2011)

We examine the leading-order semiclassical gradient corrections to the noninteracting kinetic-energy density functional of a two-dimensional Fermi gas by applying the extended Thomas-Fermi theory at finite temperature. We find a nonzero von Weizsäcker-like gradient correction, which in the high-temperature limit goes over to the functional form $(\hbar^2/24m)(\nabla\rho)^2/\rho$. Our work provides a theoretical justification for the inclusion of gradient corrections in applications of density-functional theory to inhomogeneous two-dimensional Fermi systems at any *finite* temperature.

DOI: 10.1103/PhysRevB.83.195136 PACS number(s): 71.15.Mb, 03.65.Sq, 05.30.Fk

I. INTRODUCTION

In 1966 Fower *et al.*[1] performed transport measurements on a Si-metal-oxide-semiconductor structure in which a degenerate gas of electrons was electrostatically induced. Their work demonstrated for the first time that the density of states in the n-type electron inversion layer had the expected behavior for a two-dimensional electron gas (2DEG). Since Fowler's seminal work, the exploitation of the electronic properties of III-V semiconductors has led to the realization of high-quality, high-mobility 2DEGs at the interface of epitaxially grown III-V structures, such as GaAs/AlGaAs heterostructures.[2] Through electrostatic and/or etching techniques, the 2DEG found in the III-V semiconductor interface can be manipulated to create experimental realizations of low-dimensional electron systems such as quantum wires, quantum dots, and quantum antidots.

By far, the workhorse for a theoretical understanding of the bulk electronic properties of such low-dimensional electronic systems is the zero-temperature ($T = 0$) density-functional theory (DFT) of Hohenberg, Kohn, and Sham (HKS).[3,4] The key element in the HKS approach is the definition of the kinetic energy (KE), corresponding to a system of N noninteracting fermions moving in some effective one-body potential. The HKS scheme treats the KE *exactly* at the independent particle level, and so the development of explicit, orbital-free functionals for $\mathcal{T}[\rho]$, the KE density functional, is an important objective. Ideally the appropriate functional should yield both the correct energy *and* the correct density profile.

To this end, the simplest approach for the construction of the KE density functional, $\mathcal{T}[\rho]$, is the local-density approximation (LDA), sometimes referred to as the Thomas-Fermi (TF) approximation.[5,6] In this approximation, the *known* form for KE density functional of the *uniform* electron gas is also used locally for the KE density functional of the *inhomogeneous* system. One would then expect the LDA to be applicable only in cases where the density in the system is a slowly varying function of position. In fact, this is not the case, and even in highly inhomogeneous systems, the LDA is found to work reasonably well.[7,8]

Although the LDA for the KE density leads to reasonable results for the energy, the calculated density profile in a self-consistent DFT scheme does not exhibit the desired quantum mechanical tunneling into the classically forbidden region. To overcome this issue, the so-called von Weizsäcker (vW) gradient correction,[9] $\propto (\nabla\rho)^2/\rho$, is added to the KE functional. In three dimensions the vW gradient correction can be rigorously justified within the extended TF (ETF) theory, originally developed in the context of nuclear physics.[10,11] The inclusion of the vW term leads to smooth and continuous densities while improving the quality of the KE functional by taking into account the inhomogeneity of the system.

An application of the ETF theory to 2D systems, however, leads to the conclusion that there are *no gradient corrections* to the 2D KE density functional.[12–14] This, of course, makes no physical sense since the LDA cannot be variationally exact for an inhomogeneous system. Thus in DFT applications to systems derived from the inhomogeneous 2DEG discussed above, a phenomenological approach must be taken in which a vW-like gradient correction is put in "by hand."[15] Although the vW-like correction term is entirely *ad hoc* for a 2D system, its use has been justified by the facts that (1) the KE reduces to the TF limit for slowly varying densities and (2) it allows one to represent strongly inhomogeneous densities in a quantum mechanically reasonable way.

To date, there has been no formal justification for the inclusion of a vW-like term for 2D systems at zero temperature. In this paper we establish the existence of a vW-like gradient correction to the 2D KE density functional at *finite temperatures*. Our approach parallels the earlier work of Brack,[16] in which the ETF theory was developed in the context of "hot" nuclear matter (ETFT). Given the recent work of Eschrig,[17] which aims at providing a rigorous foundation for DFT at finite temperature, the results presented in this paper are immediately relevant to future applications of $T > 0$ DFT in low-dimensional electronic systems.

This paper is organized as follows. In the next section we provide a brief review of the general ETFT approach, followed by an explicit calculation of the $T > 0$ second-order gradient correction to the 2D KE functional. In Sec. III we numerically investigate the quality of the gradient corrected functional by comparing it to known, exact results, for an isotropic 2D harmonic oscillator at finite temperature. The paper concludes in Sec. IV with a brief summary and suggestions for future investigations.

II. EXTENDED THOMAS-FERMI THEORY AT FINITE TEMPERATURE

In this section we provide a brief review of the ETFT approach. See Ref. [11] for a detailed discussion of the ETFT and the Wigner-Kirkwood semiclassical expansion.

A. Semiclassical spatial density

At the heart of the ETFT approach is the Wigner-Kirkwood (WK) semiclassical expansion of the zero temperature, diagonal Bloch density matrix (BDM), which in two dimensions is given by[11]

$$C_0(\mathbf{r};\beta) = \left(\frac{1}{\lambda}\right)^2 e^{-\beta V(\mathbf{r})} \times \left\{1 - \frac{\hbar^2\beta^2}{12m}\left[\nabla^2 V - \frac{\beta}{2}(\nabla V)^2\right] + \cdots\right\}, \quad (1)$$

where $V(\mathbf{r})$ is a local one-body potential, and for our purposes, we have shown terms only up to relative order $\hbar^2$ and $\lambda \equiv (2\pi\hbar^2\beta/m)^{1/2}$. Note that β is to be viewed as a complex parameter here, and not the inverse temperature $1/(k_B T)$. In order to incorporate finite temperatures into the WK semiclassical theory, the finite-temperature BDM is defined by[16]

$$C_T(\mathbf{r};\beta) \equiv C_0 \frac{\pi\beta k_B T}{\sin(\pi\beta k_B T)}. \quad (2)$$

The finite-temperature spatial density is then obtained from an (all two-sided) inverse Laplace transform (ILT) of the finite-temperature BDM, *viz.,*

$$\rho(\mathbf{r};T) = \mathcal{L}_\mu^{-1}\left[2\frac{C_T(\mathbf{r};\beta)}{\beta}\right], \quad (3)$$

where the factor of 2 in Eq. (3) accounts for the spin degeneracy after the spin trace has been taken, and μ has the physical significance of the chemical potential. It should be noted that if the *exact* $C_T(\mathbf{r};\beta)$ is known, then Eq. (3) will yield the exact, quantum mechanical, finite-temperature spatial density. Of course, here we are using a semiclassical expansion for $C_T(\mathbf{r};\beta)$, so the resulting $\rho(\mathbf{r};T)$ will be the semiclassical spatial density.

In what follows, we will make use of the following ILTs:

$$\mathcal{L}_\mu^{-1}\left[\beta^n e^{-\beta V}\frac{\pi k_B T}{\sin(\pi\beta k_B T)}\right] = \int_{-\infty}^{\infty}\delta^{(n)}(\tau)\frac{1}{e^{\tau/k_B T}z^{-1}+1}d\tau \quad (n \geqslant 0), \quad (4)$$

$$\mathcal{L}_\mu^{-1}\left[\beta^{-1} e^{-\beta V}\frac{\pi k_B T}{\sin(\pi\beta k_B T)}\right] = \int_0^{\infty}\frac{1}{e^{\tau/k_B T}z^{-1}+1}d\tau = k_B T\ln(1+z), \quad (5)$$

$$\mathcal{L}_\mu^{-1}\left[\beta^{-2} e^{-\beta V}\frac{\pi k_B T}{\sin(\pi\beta k_B T)}\right] = \int_0^{\infty}\frac{\tau}{e^{\tau/k_B T}z^{-1}+1}d\tau = -(k_B T)^2\mathrm{Li}_2(-z), \quad (6)$$

where $\mathrm{Li}_2(\cdot)$ is the polylog function[18] and $z \equiv \exp[(\mu - V)/k_B T]$. Using Eq. (3), along with Eqs. (4)–(6), readily leads to the following second-order expression for the finite-temperature spatial density:

$$\rho(\mathbf{r};T) = \left(\frac{mk_B T}{\pi\hbar^2}\right)\ln(1+z) - \frac{(\nabla V)^2}{24\pi k_B^2 T^2}\frac{z(z-1)}{(z+1)^3} - \frac{\nabla^2 V}{12\pi k_B T}\frac{z}{(z+1)^2} = \rho^{(0)}(\mathbf{r};T) + \rho^{(2)}(\mathbf{r};T). \quad (7)$$

The ETFT density in Eq. (7) is well defined throughout all space, with the last two terms, denoted by $\rho^{(2)}(\mathbf{r};T)$, being relative order $\hbar^2$ greater than the first term, $\rho^{(0)}(\mathbf{r};T)$. Note that in Eq. (7), for $V(\mathbf{r}) < \mu$, $z \to \infty$ *exponentially* as $T \to 0$, so that the $T \to 0$ limit is well defined only *within the classical region*; the nonanalytic behavior of the zero-temperature ETF densities at the turning point, $\mu = V(\mathbf{r})$, is well known.[11] What we find here is that the singular behavior of the $T = 0$ densities cannot be avoided by first formulating the semiclassical theory at finite temperature and then performing the $T \to 0$ limit.[19] We have, however, confirmed that the $T \to 0$ limit of Eq. (7) with $V(\mathbf{r}) < \mu$ correctly reduces to the known (albeit problematic) $T = 0$ result.[11]

B. Semiclassical KE density

The KE density may be obtained from knowledge of the finite-temperature first-order density matrix (FDM). To this end, it is useful to introduce the center-of-mass, $\mathbf{q} = (\mathbf{r} + \mathbf{r}')/2$, and relative coordinates, $\mathbf{s} = \mathbf{r} - \mathbf{r}'$, so that we may write three variants of the KE density:[20,21]

$$\mathcal{T}(\mathbf{r};T) = -\frac{\hbar^2}{2m}\left(\frac{1}{4}\nabla_{\mathbf{q}}^2 + \nabla_{\mathbf{s}}^2\right)\rho(\mathbf{q},\mathbf{s};T)|_{\mathbf{s}=0}, \quad (8)$$

$$\mathcal{T}_1(\mathbf{r};T) = \frac{\hbar^2}{2m}\left(\frac{1}{4}\nabla_{\mathbf{q}}^2 - \nabla_{\mathbf{s}}^2\right)\rho(\mathbf{q},\mathbf{s};T)|_{\mathbf{s}=0}, \quad (9)$$

$$\xi(\mathbf{r};T) = \frac{\mathcal{T}(\mathbf{r};T) + \mathcal{T}_1(\mathbf{r};T)}{2} = -\frac{\hbar^2}{2m}\nabla_{\mathbf{s}}^2\rho(\mathbf{q},\mathbf{s};T)|_{\mathbf{s}=0}. \quad (10)$$

Again, if the exact finite-temperature expression for the FDM is known, then Eqs. (8)–(10) will yield the exact, quantum mechanical finite-temperature KE density.

While all three of the above expressions for the KE density integrate to the exact same KE, $\mathcal{T}_1(\mathbf{r})$ is strictly positive definite and is therefore sometimes preferred in applications of density functional theory. It has already been shown long ago that $\mathcal{T}(\mathbf{r};T)$ and $\mathcal{T}_1(\mathbf{r};T)$ generally have oscillations exactly opposite in phase, so that their mean, $\xi(\mathbf{r};T)$, is a smooth function. In this paper we focus on $\mathcal{T}(\mathbf{r};T)$ in order to make contact with earlier theoretical work done at zero temperature, where the *exact* $\mathcal{T}(\mathbf{r};T=0)$ was investigated [see also Eq. (26) in Sec. III].[22]

The KE density in Eq. (8) may also be expressed in terms of only local quantities, *viz.,*[16]

$$\mathcal{T}(\mathbf{r};T) = -\rho(\mathbf{r};T)V(\mathbf{r}) + \mathfrak{F}(\mathbf{r};T) + T\sigma(\mathbf{r};T), \quad (11)$$

where

$$\mathfrak{F}(\mathbf{r};T) = \mu\rho(\mathbf{r};T) - \mathcal{L}_\mu^{-1}\left[\frac{C_T}{\beta^2}\right] \tag{12}$$

is the free energy density, and

$$\sigma(\mathbf{r};T) = \frac{\partial}{\partial T}\mathcal{L}_\mu^{-1}\left[\frac{C_T}{\beta^2}\right] \tag{13}$$

is the entropy density. The semiclassical approximation to $\mathcal{T}(\mathbf{r};T)$ may easily be determined to second order by employing the semiclassical approximation to $C_T(\mathbf{r};\beta)$, as in Sec. II A for the spatial density. A straightforward calculation results in the following expression for the finite-temperature, semiclassical KE density

$$\begin{aligned}\mathcal{T}(\mathbf{r};T) &= -\frac{mk_B^2T^2}{\pi\hbar^2}\mathrm{Li}_2(-z) - \frac{z(\nabla V)^2}{12\pi k_BT(z+1)^2} \\ &\quad + \frac{\nabla^2 V}{12\pi}\frac{z}{z+1} \\ &\equiv \mathcal{T}^{(0)}(\mathbf{r};T) + \mathcal{T}^{(2)}(\mathbf{r};T),\end{aligned} \tag{14}$$

where, following Eq. (7), the last two terms in Eq. (14) are denoted collectively by $\mathcal{T}^{(2)}(\mathbf{r};T)$. As in Eq. (7), the $T \to 0$ limit of Eq. (14) is well defined only within the classical region. Finally, it follows immediately from Eqs. (8) and (9) that

$$\mathcal{T}_1(\mathbf{r};T) = \mathcal{T}(\mathbf{r};T) + \frac{\hbar^2}{4m}\nabla^2\rho. \tag{15}$$

C. Second-order KE density functional

For the special case of two dimensions, the elimination of z and V in $\mathcal{T}(\mathbf{r};T)$ above, in favor of the spatial density ρ, is quite straightforward.[19,23,24] To begin we define $\tilde{V} \equiv \frac{\mu - V}{k_BT}$, so that $z = \exp(\tilde{V})$. Thus, the density [Eq. (7)] is a function of $\tilde{V}$, $\nabla\tilde{V}$ and $\nabla^2\tilde{V}$. Calculating from Eq. (7) $\nabla\rho$ and $\nabla^2\rho$ and consistently neglecting higher than second derivatives of the potential, we have $\rho = \rho(\tilde{V},\nabla\tilde{V},\nabla^2\tilde{V})$, $\nabla\rho = \nabla\rho(\cdots)$, and $\nabla^2\rho = \nabla^2\rho(\cdots)$, which can be solved for $\tilde{V}$, $\nabla\tilde{V}$, and $\nabla^2\tilde{V}$; inserting this into Eq. (14) yields the finite-temperature KE density functional up to $\mathcal{O}(\hbar^2)$, *viz.*,

$$\begin{aligned}\mathcal{T}_{\mathrm{ETFT}}[\rho] &= -A_Tk_BT\mathrm{Li}_2(1-e^{\rho/A_T}) - \frac{\hbar^2}{12m}\nabla^2\rho \\ &\quad - \frac{\hbar^2}{12m}f_1(\mathbf{r};T)\nabla^2\rho + \frac{\hbar^2}{24m}f_2(\mathbf{r};T)\frac{(\nabla\rho)^2}{\rho} \\ &= \mathcal{T}_{\mathrm{TFT}}[\rho] + \mathcal{T}^{(2)}_{\mathrm{ETFT}}[\rho],\end{aligned} \tag{16}$$

where

$$f_1(\mathbf{r};T) = \frac{\rho}{A_T(e^{\rho/A_T}-1)}, \tag{17}$$

$$f_2(\mathbf{r};T) = e^{\rho/A_T}[f_1(\mathbf{r};T)]^2, \tag{18}$$

and $A_T \equiv mk_BT/(\pi\hbar^2)$. The first term in Eq. (16) is the finite-temperature 2D TFT KE density functional, $\mathcal{T}_{\mathrm{TFT}}[\rho]$, while the other three terms represent the $\mathcal{O}(\hbar^2)$ gradient corrections. As advertised, the last term in Eq. (16) has the vW form $\sim(\nabla\rho)^2/\rho$.

An explicit expression for the $\mathcal{T}_1[\rho]$ KE functional may also be given by making use of Eq. (15), *viz.*,

$$\begin{aligned}\mathcal{T}_{1,\mathrm{ETFT}}[\rho] &= -A_Tk_BT\mathrm{Li}_2(1-e^{\rho/A_T}) + \frac{\hbar^2}{6m}\nabla^2\rho \\ &\quad - \frac{\hbar^2}{12m}f_1(\mathbf{r};T)\nabla^2\rho + \frac{\hbar^2}{24m}f_2(\mathbf{r};T)\frac{(\nabla\rho)^2}{\rho}.\end{aligned} \tag{19}$$

Recall that $\mathcal{T}_{\mathrm{ETFT}}[\rho]$ and $\mathcal{T}_{1,\mathrm{ETFT}}[\rho]$ both integrate to the same total KE for finite systems since the Laplacian term is the divergence of a vector field that vanishes at infinity and by Gauss's theorem will not contribute the KE.

To investigate the low-temperature behavior of Eqs. (16) and (19) we use

$$\lim_{\rho/A_T\to\infty}\mathrm{Li}_2(-e^{\rho/A_T}) = -\frac{1}{2}\left(\frac{\rho}{A_T}\right)^2, \tag{20}$$

along with the fact that $f_1(\mathbf{r};T) \to 0$, and $f_2(\mathbf{r};T) \to 0$ as $T \to 0$, to write

$$\mathcal{T}_{\mathrm{ETFT}}[\rho] \to \frac{\hbar^2}{2m}\left(\pi\rho^2 - \frac{1}{6}\nabla^2\rho\right) \tag{21}$$

$$\mathcal{T}_{1,\mathrm{ETFT}}[\rho] \to \frac{\hbar^2}{2m}\left(\pi\rho^2 + \frac{1}{3}\nabla^2\rho\right). \tag{22}$$

Equations (21) and (22) agree with the known results for the $T = 0$ 2D KE functionals $\mathcal{T}[\rho]$ and $\mathcal{T}_1[\rho]$, respectively.[11] As mentioned above, for physical densities, integration over $\nabla^2\rho$ vanishes. Therefore, in any practical implementation of self-consistent $T = 0$ DFT, the Laplacian term may be ignored, and we can write

$$\mathcal{T}_{\mathrm{ETFT}}[\rho] = \mathcal{T}_{1,\mathrm{ETFT}}[\rho] = \frac{\hbar^2}{2m}(\pi\rho^2) \tag{23}$$

as $T \to 0$. We see that there is no vW-like gradient correction at $T = 0$, leading to the incorrect conclusion that for an inhomogeneous 2D Fermi gas, the TF KE functional (at least to second order) is exact.[25] We would like to stress again that the nonuniqueness of the KE density does not alter the result that there are no vW-like gradient corrections at $T = 0$; the only differences between the $T = 0$ semiclassical KE densities obtained from Eqs. (8)–(10) are Laplacian terms, which, as we have already stated, are of no consequence since they vanish upon integration for physical (i.e., finite) systems.

It is readily found that as $T \to \infty$, $f_1(\mathbf{r};T) \to 1$ and $f_2(\mathbf{r};T) \to 1$, so that up to $\mathcal{O}(\hbar^2)$, the 2D KE functionals go over to

$$\mathcal{T}_{\mathrm{ETFT}}[\rho] \to \mathcal{T}_B[\rho] = k_BT\rho - \frac{\hbar^2}{6m}\nabla^2\rho + \frac{\hbar^2}{24m}\frac{(\nabla\rho)^2}{\rho} \tag{24}$$

and

$$\mathcal{T}_{1,\mathrm{ETFT}}[\rho] \to \mathcal{T}_{1,B}[\rho] = k_BT\rho + \frac{\hbar^2}{12m}\nabla^2\rho + \frac{\hbar^2}{24m}\frac{(\nabla\rho)^2}{\rho}. \tag{25}$$

Therefore, at high temperature, the second-order gradient corrections take a functional form analogous to what is found in 3D ETF, although the numerical prefactors are different. It is also interesting to note that the high-temperature

limit of the TFT term is linear in the density, $k_B T\rho$, in contrast to the quadratic dependence, $\pi\rho^2/2$, exhibited in the zero-temperature limit. We have also checked that the high-temperature limit of the 2D KE functional may be obtained by performing an analogous calculation assuming a Boltzmann, rather than a Fermi, gas.

III. COMPARISON WITH EXACT RESULTS

In a previous study, Brack and van Zyl[22] examined the $T = 0$ 2D TF KE functional by comparing its global (i.e., integrated) and local (i.e., spatially dependent) properties with the known analytical expressions for the 2D harmonic oscillator (HO) potential. They found the remarkable result that at $T = 0$, the 2D TF KE functional (*without gradient corrections*), when using the exact spatial density of the 2D HO, gives the exact quantum mechanical KE. This result is highly nontrivial because the TF functional is simply the LDA to the true KE and, therefore, cannot be variationally exact. More surprising, however, is how well the local behavior of the exact KE density is reproduced by the TF approximation, as illustrated in Fig. 3 of Ref. 22. The purpose of this section is to perform an analogous calculation for the finite-temperature KE density functionals presented in this paper. In our numerical calculations, we have scaled all energies and lengths by $\hbar\omega$, and $\ell_{\rm osc} = \sqrt{\hbar/m\omega}$, respectively. We have also restricted our attention to relatively small particle numbers, N, since it can be shown rigorously that in the large-N limit, the TF approximation becomes exact.[26]

The exact finite-temperature KE density is given by [see also Eq. (8)]

$$\mathcal{T}_{\rm exact}(\mathbf{r};T) = -\frac{1}{2}\left(\frac{1}{4}\nabla_{\mathbf{q}}^2 + \nabla_{\mathbf{s}}^2\right)\rho_{\rm exact}(\mathbf{q},\mathbf{s};T)|_{\mathbf{s}=0}, \tag{26}$$

where specializing to the case of the 2D HO,

$$\rho_{\rm exact}(\mathbf{q},\mathbf{s};T) = \frac{2}{\pi}\sum_{n=0}^{\infty}\sum_{k=0}^{\infty}(-1)^n L_n(2q^2)L_k(s^2/2)e^{-(q^2+s^2/4)} \times \frac{1}{\exp(\frac{n+1+k-\mu}{T})+1} \tag{27}$$

is the *exact* finite-temperature first-order density matrix. Putting $\mathbf{s} = 0$ in Eq. (27) gives the exact finite-temperature particle density for the 2D HO, *viz.,*

$$\rho_{\rm exact}(\mathbf{r};T) = \frac{2}{\pi}\sum_{n=0}^{\infty}\sum_{k=0}^{\infty}(-1)^n L_n(2r^2)e^{-r^2}\frac{1}{\exp(\frac{n+1+k-\mu}{T})+1}. \tag{28}$$

In Table I, we present a numerical comparison of the kinetic energies as obtained from

$$K_{\rm exact} = \int \mathcal{T}_{\rm exact}(\mathbf{r})d^2r \ \text{[cf.Eq.(23)]}, \tag{29}$$

$$K_{\rm TFT} = \int \mathcal{T}_{\rm TFT}[\rho_{\rm exact}]d^2r \ \text{[cf.Eq.(12)]}, \tag{30}$$

$$K_{\rm ETFT} = \int \mathcal{T}_{\rm ETFT}[\rho_{\rm exact}]d^2r \ \text{[cf.Eq.(12)]}, \tag{31}$$

for $N = 42$ particles, with Table II providing the same calculation for $N = 420$ particles.

TABLE I. A comparison of the total KE at various temperatures as determined from Eqs. (29–31) with $N = 42$ particles. All quantities are measured in scaled units, as discussed in the text. The largest relative percentage errors in our tabulated data are $\Delta K_{\rm TFT} \sim 0.5\%$ and $\Delta K_{\rm ETFT} \sim 0.2\%$.

T	$K_{\rm exact}$	$K_{\rm TFT}$	$K_{\rm ETFT}$
0.5	93.8984	93.4202	93.6977
0.8	97.8489	97.3152	97.7439
1.0	101.3291	100.7624	101.2613
2.0	125.9995	125.3372	125.9854
3.0	157.9066	157.2537	157.9007
4.0	193.5600	192.9616	193.5591
5.0	231.2762	230.6358	231.1417

It is clear that the TFT KE, $K_{\rm TFT}$, is always lower than the exact KE density, $K_{\rm exact}$, while the gradient corrections serve to improve the agreement with the exact result. This makes sense given that the gradient corrections take into account the curvature of the system imposed by the external potential, thereby increasing the KE of the system. It is nevertheless quite surprising how well the TFT functional does in describing the kinetic energy of the strongly inhomogeneous 2D HO at finite temperature, even for small particle numbers. From our numerical calculations, we observe that a tenfold increase in the number of particles reduces the *largest* relative percentage error by roughly a factor of ten; the better agreement between the TFT, ETFT, and the exact KE, is in keeping with the expected result that in the large-N limit, the TF approximation becomes exact.

In Figs. 1 and 2, we present the KE densities, $\mathcal{T}_{\rm exact}(\mathbf{r})$, $\mathcal{T}_{\rm TFT}[\rho]$, and $\mathcal{T}_{\rm ETFT}[\rho]$ with $N = 42$ particles, at $T = 0.2$ and 2, respectively. As in Tables I and II, the exact spatial density [Eq. (28)] has been used as input for the KE functionals.

We have focused on a small number of particles, *viz.,* $N = 42$, since deviations between the exact, TFT, and ETFT densities are more pronounced for $N \lesssim \mathcal{O}(10^2)$, particularly at low temperatures.

Figure 1 reveals several interesting aspects of the level of approximation at low temperatures. First, we note that the TFT (dot-dashed curve, black online) and the exact KE density (solid curve, red online) are almost indistinguishable within $0 < r \lesssim 3$. However, near the tail region (see figure inset), it is clear that the two KE densities are quite different; the TFT density is strictly positive definite, whereas the exact

TABLE II. As in Table I, but with $N = 420$ particles. The largest relative percentage errors in our tabulated data are $\Delta K_{\rm TFT} \sim 0.06\%$ and $\Delta K_{\rm ETFT} \sim 0.03\%$.

T	$K_{\rm exact}$	$K_{\rm TFT}$	$K_{\rm ETFT}$
0.5	2879.2573	2877.8822	2878.3566
0.8	2892.3488	2890.9642	2891.7668
1.0	2904.3701	2902.9579	2903.9484
2.0	3002.5299	3000.9349	3002.4338
3.0	3158.2817	3156.5131	3158.2465
4.0	3361.6954	3359.7806	3361.6754
5.0	3603.0235	3601.0015	3603.0076

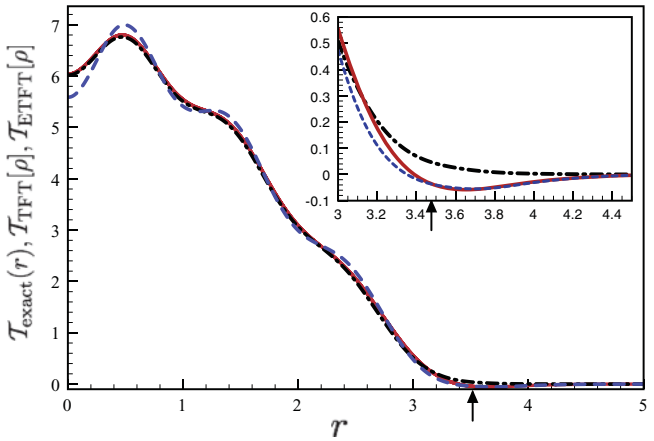

FIG. 1. (Color online) A plot of the exact [Eq. (26)] TFT, i.e., the first term in Eq. (16), and the ETFT [Eq. (16)] KE densities for $N = 42$ particles and $T = 0.2$. The solid (red online) curve is the exact KE density, the dot-dashed (black online) curve is the TFT KE density, and the dashed (blue online) curve is the ETFT KE density. Inset: Magnification of the tail region, where deviations between the three curves are most pronounced. The arrow indicates the classical turning point. Scaled units are used as discussed in the text.

KE density falls below zero, before coalescing with the TFT density for $r \gtrsim 4.5$. The ETFT KE density (dashed curve, blue online), on the other hand, does a relatively poor job of quantitatively capturing the behavior of the exact KE density in the interior, but for the tail region more accurately reproduces the exact result. Indeed, for $r \gtrsim 3.5$, the ETFT and exact KE densities are indistinguishable on the scale of the inset. Moreover, in spite of the differences between the exact and ETFT densities for $r \lesssim 3$, the ETFT is still a better approximation for the total KE, as evidenced by the data presented in Table I. Therefore, while the gradient corrections are important for improving the total (i.e., integrated) KE, they are essential for describing the correct low-

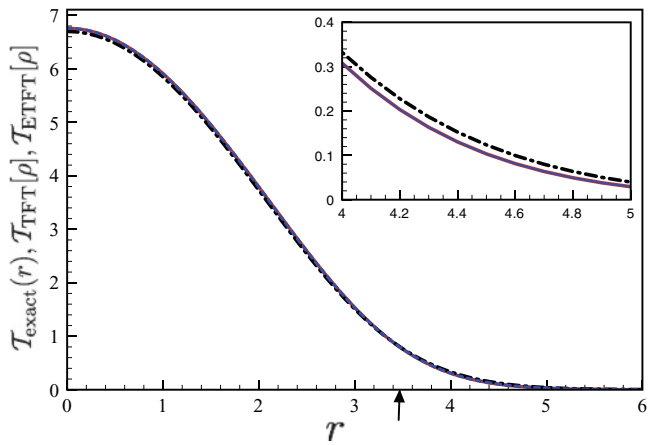

FIG. 2. (Color online) As in Fig. 1, but with $T = 2.0$. Note that at this temperature, the shell oscillations are already completely washed away. Inset: Magnification of the tail region, clearly illustrating that the exact (solid curve, red online) and ETFT (dashed curve, blue online) curves are indistinguishable on the scale of the plot. The arrow indicates the classical turning point.

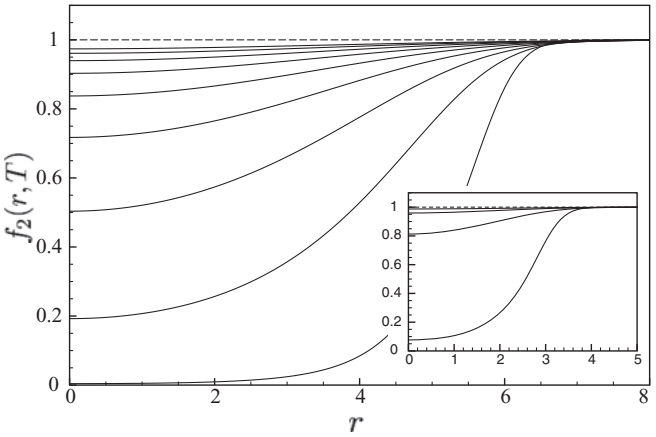

FIG. 3. A plot of the coefficient of the von Weizsäcker term [Eq. (18)] for $N = 420$ particles. The curves correspond, from lowest to highest, to $T = 2$ and 18, respectively, in steps of $\Delta T = 2$. Note that by $T = 18$, $f_2(\mathbf{r}; T)$ is already approaching its Boltzmann value, $f_2(\mathbf{r}; T) = 1$, represented by the dashed line. Inset: As in the main figure, but for $N = 42$ particles at temperatures $T = 1,3,5,7$. Scaled units have been used, as discussed in the text.

temperature behavior of the exact KE past the classical turning point.

Figure 2 presents the same data as in Fig. 1, but with $T = 2.0$. At this temperature, the shell oscillations are already completely washed out, and the exact and ETFT KE densities are *indistinguishable* from each other, including the tail region; in the inset, there are actually three curves plotted, but the difference between the solid (red online) and dashed (blue online) curves cannot be resolved. Thus, at temperatures for which the shell effects are absent (i.e., $T \gtrsim 1$), the ETFT is an excellent approximation to the exact finite-temperature KE density. Near the tail region, we see that the TFT KE density (dot-dashed curve, black online) is consistently too large, thereby emphasizing the importance of the gradient corrections for a faithful description of the local behavior of the exact KE density, even for small particle numbers.

Finally, in Fig. 3, we illustrate the temperature and spatial dependence of the vW coefficient, $f_2(\mathbf{r}; T)$ given by Eq. (18), for $N = 420$ particles and $N = 42$ (inset). As the temperature is increased, we see that the vW coefficient approaches the constant value $f_2(\mathbf{r}; T) = 1$, confirming our analytical results above for the Boltzmann regime. Figure 3 establishes that $T \gtrsim 18$ is a sufficiently high temperature for the $N = 420$ particle system to be treated as Boltzmann gas. The inset illustrates the expected result that for smaller particle numbers, one enters the Boltzmann regime at much lower temperatures.

IV. CONCLUSIONS AND OUTLOOK

We have provided a formal justification for the inclusion of gradient corrections to the 2D KE density functional of an ideal Fermi gas at finite temperatures. Our numerical calculations have examined the quality of the TFT and ETFT functionals by comparing them against exact, analytical results for the 2D HO potential. We find that gradient corrections lead to an improved agreement for total KE when compared to the TFT approximation and are necessary to correctly reproduce the

quantum mechanical tunneling into the classically forbidden region exhibited by the exact KE density. Unfortunately, the nonanalytic behavior of the $T = 0$ semiclassical densities at the classical turning point cannot be remedied within the present formalism.

An extension of this work would be to develop the finite-temperature Dirac exchange functional, which could then be used in a fully self-consistent, finite-temperature Thomas-Fermi-Dirac von Weizsäcker (TFDW) DFT calculation similar to what has already been done at $T = 0$ for low-dimensional Fermi systems.[15] It would be interesting to see whether the optimal, *ad hoc*, $T = 0$ vW coefficient of $1/8$ could be motivated from a finite-temperature self-consistent TFDW calculation.

Finally, we wish to point out that the results presented here may also find relevance in current experiments on ultracold, trapped Fermi gases, in which interatomic interactions may be tuned from essentially zero, to very strong, via the Feshbach resonance.[27] It is possible that the low-temperature shell oscillations, and their suppression as the temperature is increased, may be directly observable in cold atoms experiments on low-dimensional systems.

ACKNOWLEDGMENTS

B. P. van Zyl acknowledges financial support from the Natural Sciences and Engineering Research Council (NSERC) of Canada through the Discovery Grants program. A. Farrell acknowledges the NSERC Undergraduate Student Research Awards (USRA) program for additional financial support.

[1] A. B. Fowler, F. F. Fang, W. E. Howard, and P. J. Stiles, Phys. Rev. Lett. **16**, 901 (1966).
[2] H. Ehrenreich and D. Turnbull, editors, *Solid State Physics: Semiconductor Heterostructures and Nanostructures* (Academic Press, New York, 1991).
[3] P. Hohenberg and W. Kohn, Phys. Rev. B **136**, B864 (1964).
[4] W. Kohn and K. Sham, Phys. Rev. B **140**, A1133 (1965).
[5] L. H. Thomas, Proc. Cambridge Philos. Soc. **3**, 542 (1927).
[6] E. Fermi, Rend. Acad. Naz. Lincei **6**, 602 (1927).
[7] H. Eschrig, *Fundamentals of Density Functional Theory* (Teubner, Stuttgart, 1996).
[8] R. M. Driezler and E. K.U. Gross, *Density Functional Theory: An Approach to the Quantum Many-Body Problem* (Springer-Verlag, Berlin, 1990).
[9] C. F. von Weizsäcker, Z. Phys. **96**, 431 (1935).
[10] The vW correction to the KE density functional, and higher-order gradient corrections obtained from ETF, are sometimes referred to as conventional gradient expansions (CGEs). The generalized gradient expansion (GGA) offers an alternative approach for capturing the corrections to the LDA. The underlying connection, and differences between, the CGE and GGA can be found in, e.g., E. Wang and E. Carter, *Theoretical Methods in Condensed Phase Chemistry*, in the book series *Progress in Theoretical Chemistry and Physics*, edited by S. D. Schwartz (Kluwer, Dordrecht, 2000), p. 117.
[11] M. Brack and R. K. Bhaduri, *Semiclassical Physics*, Frontiers in Physics, Vol. 96 (Addison-Wesley, Reading, MA, 2003).
[12] A. Holas, P. M. Kozlowski, and N. H. March, J. Phys. A: Math. Gen. **24**, 4249 (1991).
[13] L. Salasnich, J. Phys. A: Math. Theor. **40**, 9987 (2007).
[14] M. Koivisto and M. J. Stott, Phys. Rev. B **76**, 195103 (2007).
[15] B. P. van Zyl and E. Zaremba, Phys. Rev. B **59**, 2079 (1999); Physica E **6**, 423 (2000); B. P. van Zyl, E. Zaremba, and D. A. W. Hutchinson, Phys. Rev. B **61**, 2107 (2000); B. P. van Zyl and E. Zaremba, *ibid.* **63**, 245317 (2001).
[16] M. Brack, Phys. Rev. Lett. **53**, 119 (1984).
[17] H. Eschrig, Phys. Rev. B **82**, 205120 (2010).
[18] The polylog function, $\mathrm{Li}_2(\cdot)$ is identical to the Fermi integral, $F_\xi = \int_0^\infty \frac{\tau^\xi}{1+\exp(\tau-\eta)} d\tau$, with $\xi = 1$. See Ref. 11 for details.
[19] J. Bartel, M. Brack, and M. Durand, Nucl. Phys. A **445**, 263 (1985).
[20] R. J. Lombard, D. Mas, and S. A. Moszkowski, J. Phys. G: Nucl. Part. Phys. **17**, 455 (1991); E. Sim, J. Larkin, K. Burke, and C. W. Bock, J. Chem. Phys. **118**, 8140 (2003).
[21] P. Shea and B. P. van Zyl, J. Phys. A: Math. Theor. **40**, 10589 (2007).
[22] M. Brack and B. P. van Zyl, Phys. Rev. Lett. **86**, 1574 (2001).
[23] The functional inversion procedure used here is not possible in three dimensions because of the complicated dependence of z and V on the spatial density. See Ref. 19 for a detailed derivation of the elimination of z and V in favor of ρ to obtain the 3D finite-temperature KE functional.
[24] P. Ring and P. Schuck, *The Nuclear Many-Body Problem* (Springer-Verlag, Berlin, 2004).
[25] While we have not presented the cumbersome calculation here, the more general result that *all* finite-temperature gradient corrections vanish at $T = 0$ has also been established.
[26] B. P. van Zyl, R. K. Bhaduri, A. Suzuki, and M. Brack, Rev. A **67**, 023609 (2003).
[27] Wenhui Li, G. B. Partridge, Y. A. Liao, and R. G. Hulet, Int. J. Mod. Phys. B **23**, 3195 (2009).